Title

Luminescent Solar Concentration with Semiconductor Nanorods and Transfer-Printed Micro-Silicon Solar Cells

Journal

ACS Nano, 8(1)

ISSN

1936-0851

Authors

Bronstein, Noah D.
Li, Lanfang
Xu, Lu
et al.

Publication Date

2014-01-28

Luminescent Solar Concentration with Semiconductor Nanorods and Transfer-Printed Micro-Silicon Solar Cells

Noah D. Bronstein,[†,∥] Lanfang Li,[‡,§,∥] Lu Xu,[§] Yuan Yao,[§] Vivian E. Ferry,[†,⊥] A. Paul Alivisatos,[†,⊥,*] and Ralph G. Nuzzo[‡,§,*]

[†]Department of Chemistry, University of California, Berkeley, California 94720, United States, [‡]Department of Materials Science and Engineering and [§]Department of Chemistry, Frederick Seitz Materials Research Laboratory, University of Illinois at Urbana—Champaign, Urbana, Illinois 61801, United States, and [⊥]Materials Science Division, Lawrence Berkeley National Laboratory, Berkeley, California 94720, United States. [∥]These authors contributed equally to this work.

ABSTRACT We utilize CdSe/CdS seeded nanorods as a tunable lumophore for luminescent concentration. Transfer-printed, ultrathin crystalline Si solar cells are embedded directly into the luminescent concentrator, allowing the study of luminescent concentrators with an area over 5000 times the area of the solar cell. By increasing the size of the CdS rod with respect to the luminescent CdSe seed, the reabsorption of propagating photons is dramatically reduced. At long luminescence propagation distances, this reduced reabsorption can overcome the diminished quantum yield inherent to the larger semiconductor structures, which is studied with lifetime spectroscopy. A Monte Carlo ray tracing model is developed to explain the performance of the luminescent concentrator and is then used as a design tool to determine the effect of luminescence trapping on the concentration of light using both CdSe/CdS nanorods and a model organic dye. We design an efficient luminescence trapping structure that should allow the luminescent concentrator based on CdSe/CdS nanorods to operate in the high-concentration regime.

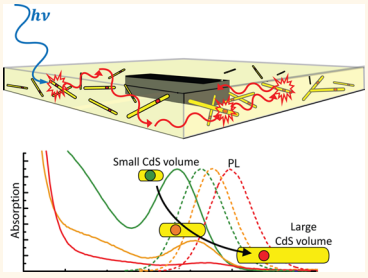

KEYWORDS: photovoltaic · quantum dot · nanorod · transfer printing · luminescent concentration · light trapping · micro-silicon

In this study, we examine the performance of luminescent solar concentrators utilizing a semiconductor nanocrystal heterostructure lumophore in which it is possible to separately tune the composition, volume, and band gaps of the absorbing and emitting portions. In this way, it is possible to systematically control the Stokes shift of the lumophore and the characteristic length scale over which light concentration can be achieved. The highly developed CdSe/CdS seeded nanorod system is used to study the propagation of light inside the concentrator with this unique class of lumophore. Success with this well-understood system may encourage the development of lower band gap heterostructure lumophores better matched to the solar spectrum.

Luminescent concentration for photovoltaic energy production has long been studied as a means to concentrate both direct sunlight and diffuse light onto high-efficiency solar cells.[1,2] A luminescent solar concentrator (LSC) typically consists of a luminescent dye, or lumophore, embedded in a polymer sheet with a high-performance solar cell attached at the side. In such a device, sunlight is absorbed in a lumophore, emitted into the waveguide modes of the polymer sheet, and directed to a photovoltaic cell where it is absorbed and converted to electricity. Since the area of the polymer sheet is greater than the area of the photovoltaic cell, concentration of the solar photon flux is achieved. In addition, high-energy photons which are typically difficult to utilize in a photovoltaic cell are down-converted to a more efficiently utilized wavelength.

Thermodynamically, these devices operate by harnessing the Stokes shift of the lumophore.[3,4] The thermodynamic limit for photon concentration increases exponentially with the Stokes shift of the lumophore. For example, the thermodynamic concentration limit for a lumophore absorbing at 500 nm and emitting at 600 nm is around 11 500 000. In contrast, a perfect lens can concentrate sunlight by a factor of 46 200, and practical concentrator systems typically operate at concentration factors of a few hundred to a few thousand due to difficulties

* Address correspondence to alivis@berkeley.edu, r-nuzzo@illinois.edu.

Received for review August 23, 2013 and accepted December 19, 2013.

Published online December 19, 2013
10.1021/nn404418h

in tracking precision, lens precision, and thermal degradation of photovoltaic performance.[5] The luminescent solar concentrator avoids all of these problems: it requires no lenses and no trackers, and the heat generation from high-energy photons is distributed in the LSC instead of being concentrated on the photovoltaic cell. In the thermodynamic limit, all of the energy lost to the Stokes shift is recovered as increased voltage from the concentration of photons onto the photovoltaic cell. In practice, such high concentration is elusive and LSC devices have to date been limited to concentration factors around 10.[6]

The disparity between ideal and real luminescent solar concentrators is due to incomplete trapping of luminesced light and nonunity fluorescence quantum yields.[7,8] The root of this problem is excessive overlap between lumophore absorption and emission spectra. As a luminesced photon travels through the LSC, it may be reabsorbed by other lumophores. Every reabsorption event presents an opportunity for loss, such as nonradiative decay or emission into the escape cone. For this reason, LSC concentration ratios plateau long before the thermodynamic limit. This effect has been shown in recent work with inorganic lumophores,[9,10] organic lumophores in microgeometries with transfer-printed silicon[11,12] and GaAs solar cells,[13] as well as studied by numerical modeling.[14−16] In order for luminescent concentrators to approach their thermodynamic limits, the luminesced light must be trapped in the polymer and directed onto the solar cell. For the most effective light trapping, a lumophore with a narrow emission spectrum and a large Stokes shift is required. Studies of light trapping have been limited by a dearth of dyes meeting these criteria.[17,18] In summary, approaching the thermodynamic concentration limit will require a lumophore with large Stokes shift, high quantum yield, minimal overlap between absorption and emission, and a narrow emission spectrum.

Semiconductor nanocrystals[19,20] have been considered as lumophores in LSCs due to their broad absorption spectra, high fluorescent quantum yields,[21] resistance to photobleaching,[22] and tunable absorption and emission spectra. However, they have not been systematically tuned in past LSC studies to reduce the absorption/emission overlap. Single-component nanocrystals such as CdSe have significant overlap between their absorption and emission spectra and have small Stokes shifts. Core/shell materials such as CdSe/CdS utilize the separate absorption spectra of the two components to achieve lower reabsorption. While the absorption−emission overlap decreases with increasing CdS shell thickness, so does the luminescent quantum yield. Bomm *et al.* performed a systematic study of a quantum dot LSC using CdSe/CdS core−shell quantum dots and obtained a moderate concentration ratio.[21] Additionally, since the reabsorption is reduced by increasing the CdS shell size, a very large shell is needed. Progress has been made in the growth of thick CdS shells onto CdSe seeds, but shell thicknesses have so far been limited to around 10 nm.[23−25]

In this study, we examine the performance of luminescent solar concentrators utilizing semiconductor nanocrystal heterostructure lumophores meeting all four of the above requirements: the CdSe/CdS seeded nanorod. Similar to CdSe/CdS core−shell particles, there is a small CdSe core with a large volume of CdS grown on top. However, it is possible to grow much larger volumes of CdS in the nanorod geometry than in the core−shell geometry, resulting in significantly reduced absorption−emission overlap and long propagation distances in the waveguide. In addition, seeded nanorods have routinely achieved luminescent quantum yields of 30−80% and excellent air stability compared to spherical core−shell particles. Past studies of CdSe/CdS seeded nanorods for luminescent concentration have focused on utilizing the polarized emission of self-assembled vertical arrays of nanorods to limit the escape of luminesced photons.[26] In this study, we instead explore the tunable geometry of the CdSe/CdS nanorod system and demonstrate that large nanorods do indeed reduce the reabsorption of luminesced photons as they travel through the film. Additionally, we accurately model the experimental data from first-principles with a Monte Carlo ray tracing simulation and use the simulation to illustrate paths to the high-concentration regime. We describe a photonic light-trapping structure that, based on predictions of theory, reflects over 99% of luminesced photons from the nanorods. The same light-trapping strategy used on a model organic dye, dicyanomethylene, results in a trapping efficiency of only 95% due to the broad emission linewidth of the organic dye. Comparison of the nanorods and organic dye in the Monte Carlo model shows that efficient light trapping allows the nanorods to achieve higher concentration than their organic counterparts. Finally, with good light trapping in place, an increase in the volume of the nanorod results in an increase in the concentration of photons.

RESULTS AND DISCUSSION

Synthesis and Characterization of CdSe/CdS Nanorods. Figure 1a−f shows TEM micrographs of a series of nanorods that were synthesized, keeping the CdSe seed a constant 2.5 nm diameter and increasing the final rod size from 4.1 nm × 8.8 nm in the smallest case to 9.3 nm × 78 nm in the largest case. Synthetic details can be found in Supporting Information. As shown in Figure 1g, longer and thicker rods result in a lower volume fraction of CdSe and thus lower absorption at wavelengths longer than 500 nm. Additionally, the absorption spectrum is measured in transmission mode, allowing the spectra of the largest nanorods to display scattering at energies lower than the excitonic absorption feature at 580−620 nm. Increasing nanorod size

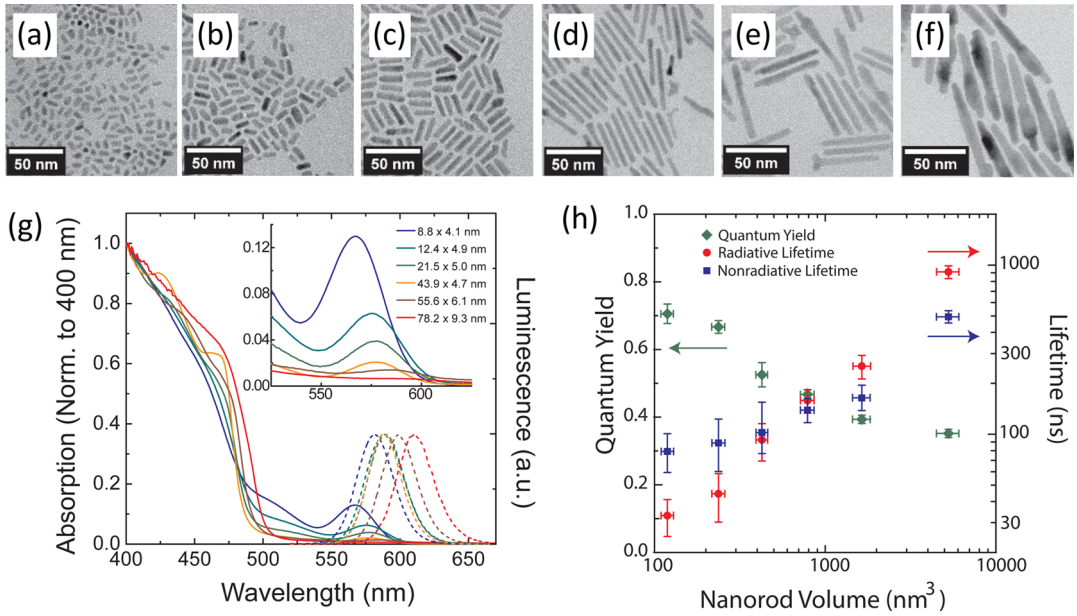

Figure 1. Characterization of CdSe/CdS seeded nanorods with different CdS volumes. (a–f) Typical TEM micrographs, (g) absorption and photoluminescence spectra, and (h) luminescent quantum yield from 380 to 450 nm and radiative and nonradiative lifetimes. Larger rods show larger Stokes shifts, reduced absorption of the luminescent wavelengths, reduced luminescent quantum yields, and longer radiative and nonradiative lifetimes with increased CdS rod volume. The error bars in (h) represent the 95% confidence interval.

results in a red shift of the luminescence peak from 570 nm in the smallest rods to 610 nm in the largest nanorods due to a reduction in quantum confinement. Figure 1h shows the relationship between nanorod size, luminescent quantum yield, radiative lifetime, and nonradiative lifetime. Both luminescence lifetime and quantum yield were measured in solution phase. Radiative (τ_{rad}) and nonradiative (τ_{nr}) lifetimes are determined from the measured photoluminescence lifetime (τ_{meas}) and the luminescent quantum yield (QY) by the formula

$$QY = \frac{\tau_{meas}}{\tau_{rad}} = \frac{\tau_{nr}}{\tau_{nr} + \tau_{rad}} \quad (1)$$

The radiative lifetime of the nanorods increases linearly with increasing nanorod volume from 33 ± 8 ns for the smallest nanorods to 911 ± 80 ns for the largest nanorods in this study. Similar results have been reported recently.[27] The increase in radiative lifetime with increasing nanorod volume is mitigated by an increase in the nonradiative lifetime from 79 ± 19 ns for the smallest nanorods to 494 ± 41 ns for the largest nanorods. As a result, the quantum yield does not decrease as much as one might expect, dropping from 71 ± 3% for the smallest nanorods to 35 ± 1% for the largest nanorods.

LSC Design and Fabrication. One of the main challenges in fabricating a LSC with inorganic nanoparticles is dispersing them in a polymer matrix without agglomeration or quenching of their luminescence. Earlier work by Lee *et al.* demonstrated that poly(lauryl methacrylate) (LMA) with a high concentration of cross-linker ethylene glycol dimethacrylate (EDGMA) may be used to form well-dispersed quantum dot-polymer composites.[28] A similar procedure has been utilized to successfully fabricate LSCs incorporating quantum dots.[29] Here, we modify the formulation by reducing the cross-linker concentration to avoid stress-induced tears in the film. We also use UV photoinitiated polymerization to promote fast polymerization kinetics and mitigate agglomeration of the nanorods. The absorption spectra, luminescence spectra, and luminescence quantum yield of the nanorods were unchanged upon integration into the polymer.

To study the performance of the LSC, a transfer-printed micro-silicon photovoltaic cell[30] with thermal oxide passivation on the top and side walls[31] was embedded in a 30 μm thick polymer/nanorod composite, all supported by a 180 μm thick quartz sheet. The best performance is attained when photons can propagate long distances in the waveguide, which requires excellent reflectivity of the waveguide surfaces. For example, in a LSC with a thickness of 210 μm and a radius of 20 mm, photons traveling from the edge of the sheet must be reflected up to 100 times without appreciable loss. To obtain highly reflective waveguide surfaces, the LSC polymer sheet was formed by capillary infilling of an air gap between two smooth quartz plates, as depicted in Figure 2a. The supporting substrate was treated with an acrylate functional silane to promote adhesion, while the top plate was treated with a fluorosilane to facilitate delamination. The liquid film was then cured under UV illumination, and the top plate was removed, leaving the μ-cells embedded in a polymer sheet with a flat top surface. A schematic of the completed device is shown in Figure 2b. It is also possible to support the LSC

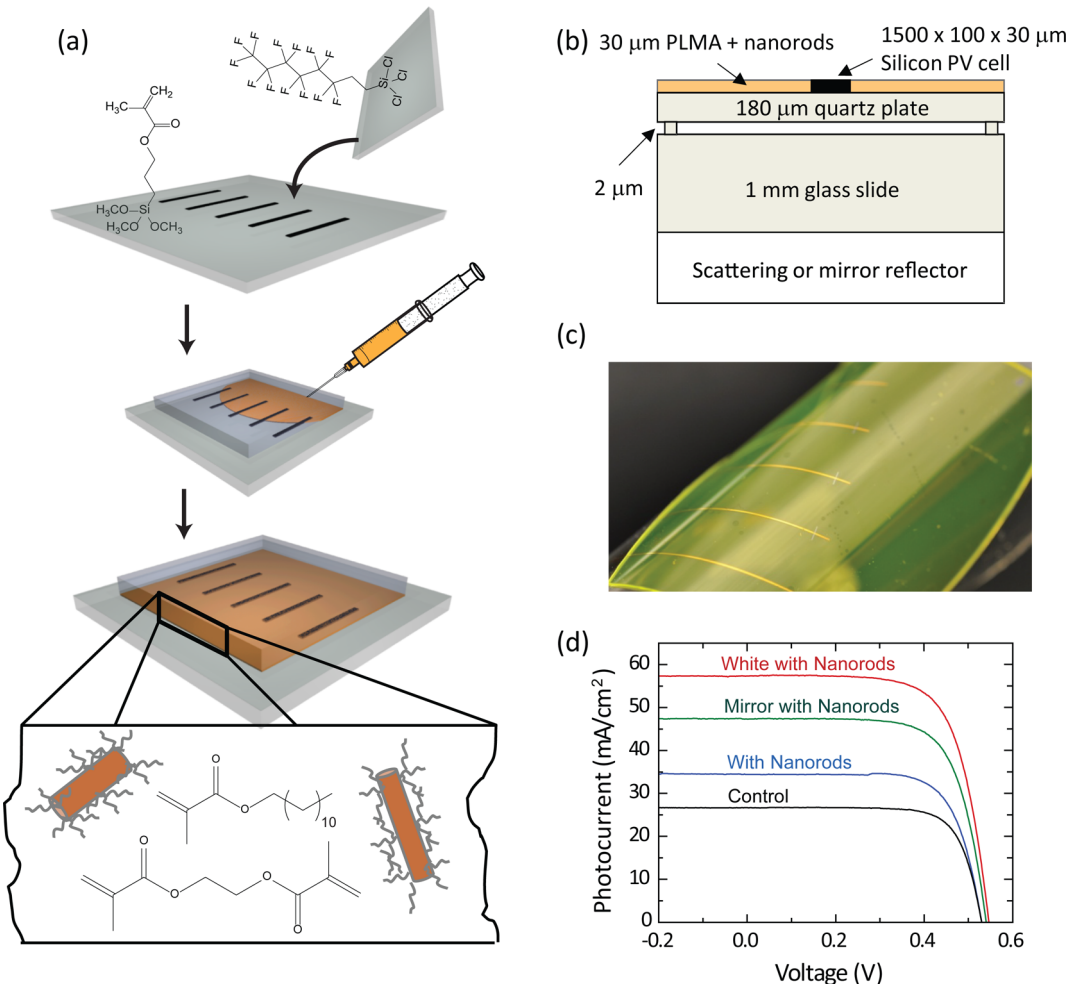

Figure 2. (a) Schematic of the fabrication of the LSC device and integration with a solar cell, (b) vertical cross section schematic of the LSC, and (c) photograph of a fabricated device on a flexible plastic substrate. (d) Current–voltage plot shows performance characteristics of a micro-silicon cell integrated with the LSC.

device with flexible plastic, as shown in Figure 2c. Fabrication details are given in the Experimental Section.

The LSC devices were characterized by measuring the photovoltaic response of an embedded solar cell under AM1.5G illumination. Four typical I-V curves are shown in Figure 2d. The control device has a black absorbing back surface and no nanorods in the LSC polymer, resulting in a short circuit current density (J_{sc}) of 26.7 mA·cm^{-2}. The introduction of nanorods results in an increase in the short circuit current density (J_{sc} = 34.4 mA·cm^{-2}). The addition of both mirrored silver and white scattering back surfaces further increases the short circuit current density (to 47.3 and 57.3 mA/cm^{-2}, respectively) and results in small increases in the open circuit voltage. While it should be noted that these curves do not represent the best performance achieved in this study, the electronic properties of the cells remain consistent regardless of the LSC fabrication process, as evidenced by the consistent fill factor of around 0.7 for all devices.

Effects of Nanorod Loading on LSC Performance. Figure 3a shows the performance of the LSC as a function of nanorod loading. The concentration as a function of incident wavelength is measured by taking external quantum efficiency measurements with the beam illuminating a 7 mm radius spot on the LSC and normalizing to the performance of the micro solar cell measured at 600 nm in the same geometry without any lumophore and without a reflective back surface. The device with no nanorods (OD = 0) but with a reflective back surface is shown for comparison. The concentration can exceed 1 without nanorods but with a reflective back surface due to the angular spread of the light source in the measurement. Photons that enter the LSC at oblique angles near the solar cell can be reflected onto the solar cell. To maximize the probability that a photon traveling through the waveguide is absorbed in the photovoltaic cell, the polymer must not be much thicker than the photovoltaic cell itself, which is 30 μm. To achieve optical density of 1 in the film, approximately 0.3% of the polymer volume must be displaced by nanorods.[32] Increasing the nanorod loading initially increases the concentration of light from the blue region of the spectrum, where the nanorods absorb,

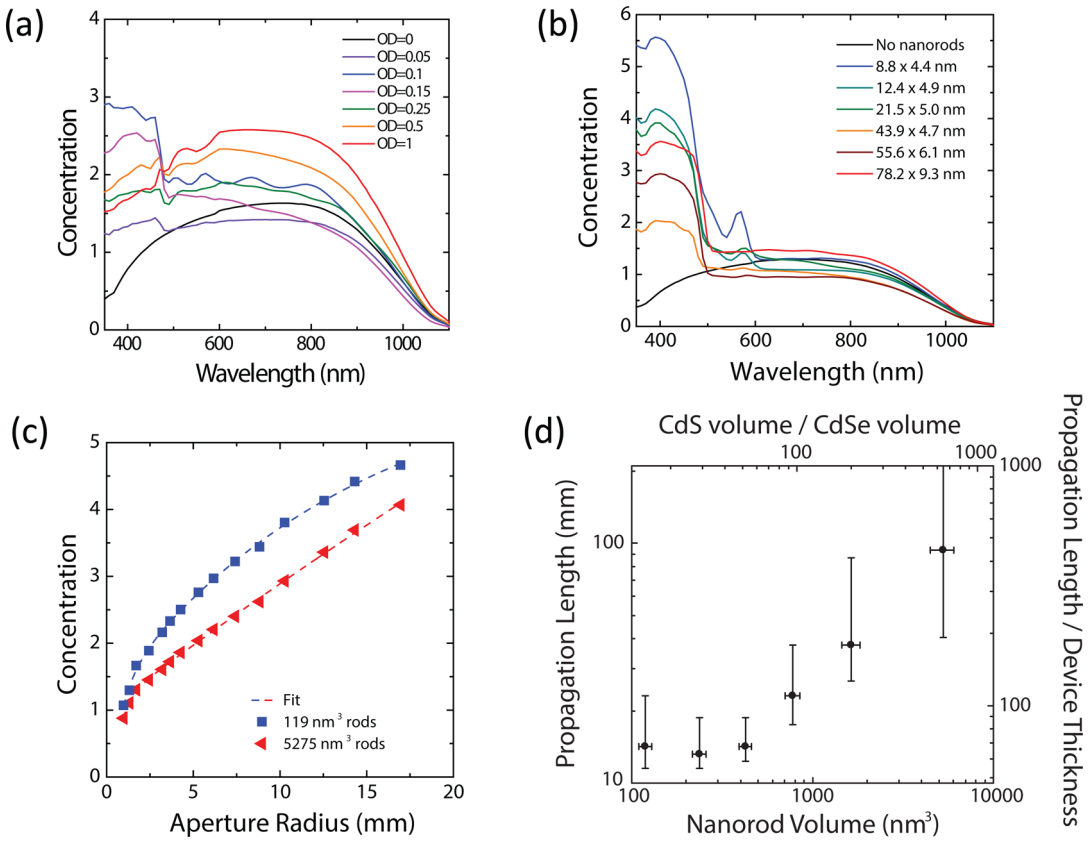

Figure 3. Optimization of the nanorod optical density (a) shows that, at too high of a nanoparticle loading in the polymer, the nanoparticles agglomerate and scattering reduces the concentration of luminesced light over long distances. Increasing CdS nanorod volume, optical density at 450 nm is held constant at 0.1 by reducing the total number of nanoparticles. At a 7 mm device radius, the concentration as a function of wavelength (b) shows little scattering for all nanorod sizes and higher concentration for the smallest particles, which have the highest luminescent quantum yields. The concentration of blue light as a function of aperture radius (c) shows that, with optical density held constant, larger nanorods result in longer propagation distances (d) for luminesced photons. The vertical error bars in (d) represent curve fit 95% confidence interval, and the horizontal error bars represent the 95% confidence interval of the nanorod volume.

without concentrating light from the red region of the spectrum, where the nanorods do not absorb. Using a EGDMA cross-linker concentration of 10% yielded minimal scattering at optical density up to 0.1 at 450 nm. However, above an optical density of 0.1, concentration of blue light decreases and concentration of red light increases because of the scattering of light in the waveguide, likely as a result of nanoparticle agglomeration. Under the photoinitiated polymerization scheme, increasing the EGDMA cross-linker content to 20% allows for kinetic control of the polymer matrix formation, keeping the nanoparticles well-dispersed as evidenced by high optical clarity. These films, however, have a tendency to tear and crack, presumably due to internal stress.

Effects of Nanorod Size on LSC Performance. The performance of the LSC as a function of nanorod size was also investigated. Optical density for these devices was held to around 0.1 at 450 nm to avoid the scattering apparent at higher loadings. This is accomplished by holding the volume fraction of CdS nearly constant. Large nanorods, then, are incorporated in fewer numbers than small nanorods. Absorption spectra of the films can be found in Supporting Information. Figure 3b shows the concentration as a function of wavelength for the different nanorod sizes. In all cases, the concentration of blue photons in the device follows the absorption spectrum of the nanorods; the concentration of red photons is suppressed in each case, confirming minimal scattering of light in the LSC sheet.

The propagation of photons inside the waveguide was characterized by illumination in a solar simulator with an aperture controlling the illumination area. A blue band-pass filter centered at 405 nm is used to isolate the luminescence of the nanorods from scattered red light. A circular aperture is centered on the silicon photovoltaic cell and the photocurrent measured as a function of aperture radius. Figure 3c shows the results for the largest and smallest nanorods. The smallest nanorods show concentration factors that increase rapidly at small radii but begin to asymptote at larger radii. In contrast, the larger nanorods show concentration factors that increase nearly linearly with increasing radius. The propagation of photons inside the waveguide can be approximated as an exponential decay with a characteristic length scale defined as the

propagation length. Allowing for a short-propagating population of scattered photons and a long-propagating population of luminesced photons, the photocurrent is fit to the equation

$$J_{photo}(r) = J_{max} - A_1 \exp\left(-\frac{r}{L_1}\right) - A_2 \exp\left(-\frac{r}{L_2}\right) \quad (2)$$

where $J_{photo}(r)$ is the measured photocurrent density at an aperture radius r and the following parameters are a result of the curve fit: J_{max} is the photocurrent density at infinite device size, L_1 and L_2 are the propagation lengths for scattered and luminesced photons, respectively, with their associated magnitudes A_1 and A_2. This model is reasonable because the population of scattered photons must be generated on one pass through the LSC, requiring a characteristic scattering length on the order of the thickness of the LSC. As a result, scattered photons only travel a few hundred micrometers. In contrast, the luminesced photons have been shifted from their incident wavelength to the luminescent wavelength, allowing for different length scales for generation and propagation. The propagation length of the luminesced photons, plotted in Figure 3d, shows increasing propagation length with increasing nanorod volume due to the reduced reabsorption from the CdSe seed.

As a result of the limited optical density of the films, a reflective back surface is required to increase the absorption path length. In this study, a black anodized aluminum surface, a silver mirror, and a scattering white Spectralon surface were used. The propagation lengths in Figure 3d are not significantly different for the different back surfaces (see Supporting Information). A black back surface allows 1 pass for absorption, a mirror back surface allows 2 passes, and a scattering surface allows 2.2 passes for a polymer with refractive index of 1.4, as the oblique rays bend back toward normal upon refraction into the polymer (see Supporting Information). While this optical path length enhancement is less than the $4n^2$ Yablonovitch scattering limit of 7.8, that limit is only achieved by continual randomization of photons within the polymer, which would eliminate the long-traveling waveguide modes.[33,34] While it is still possible in theory to achieve luminescent concentration beyond the scattering limit in such a circumstance with the application of perfect light trapping, continuous randomization would place an extraordinary burden on the luminescent quantum yield of the lumophore and reflectivity of all surfaces. This logic also applies to highly scattering lumophores such as nanorod agglomerates and is the reason that agglomeration is detrimental to device performance.

Monte Carlo Ray Tracing Simulation. To explore the potential for improving the performance of the LSC device, a Monte Carlo ray tracing simulation was developed. These models have been previously shown to be accurate if accurate physical parameters are used.[7,8,15,16,21,35] In this case, the simulation was performed utilizing measured values for the absorption spectrum of the nanorods in solution, nanoparticle loading in the film, luminescent quantum yield of the nanoparticles, and luminescence spectra of the nanoparticles. Absorption in the thin silicon cell is calculated with the finite-difference time domain (FDTD) method, assuming every absorbed photon is collected as current.[36] Reflections and refractions are calculated at every interface of the LSC with Fresnel coefficients. A detailed description of both the Monte Carlo simulation and the FDTD method can be found in the Supporting Information, and the results are shown against experiments in Figure 4a. As a result of the excellent agreement between the model and the experimental data, the simulation was used to search for a path to the high-concentration regime.

The Monte Carlo simulation shows that, at larger illumination spot sizes, the larger nanorods outperform the smaller nanorods due to the relatively free propagation of photons inside the LSC despite the lower luminescent quantum yield of the larger nanorods. At the experimentally achieved illumination radius of 18 mm, the area of the LSC is already 6800 times the area of the micro solar cell and a vast majority (over 99%) of the luminesced photons are eventually lost either out the side or out the top of the sheet. Therefore, trapping the luminesced light may have a much larger effect than simply increasing the size of the sheet. Light trapping at the side of the sheet could be accomplished by the addition of a mirror on the edge. Light trapping on the top is a more complicated matter because it must allow blue photons to pass through at normal incidence, and must reflect luminesced red photons at every angle as they impinge on the top surface of the LSC sheet. This could be accomplished by the addition of a photonic structure such as a 1-D Bragg mirror.

The reflectance band of the Bragg mirror must contain the luminescence spectrum of the lumophore at angles ranging from normal incidence up to the angle of total internal reflection. Further, the dielectric materials used in the Bragg mirror must have a band gap higher than the CdS absorber, and they must have low subgap absorption. A Bragg reflector was designed for each nanorod emission spectrum, optimizing for the highest reflectance averaged over a constant brightness hemisphere and the emission spectrum of the nanorods (details in Supporting Information). In addition, the same Bragg reflector optimization strategy was performed for dicyanomethylene (DCM), a model organic dye. Figure 4b shows the reflectivity spectrum for the Bragg mirror at normal incidence and immediately before the angle of total internal reflection, with the emission spectra of a nanorod sample and DCM superimposed for comparison. The narrow emission line width of the nanorods allows angle- and wavelength-averaged reflectivity exceeding 99% in all

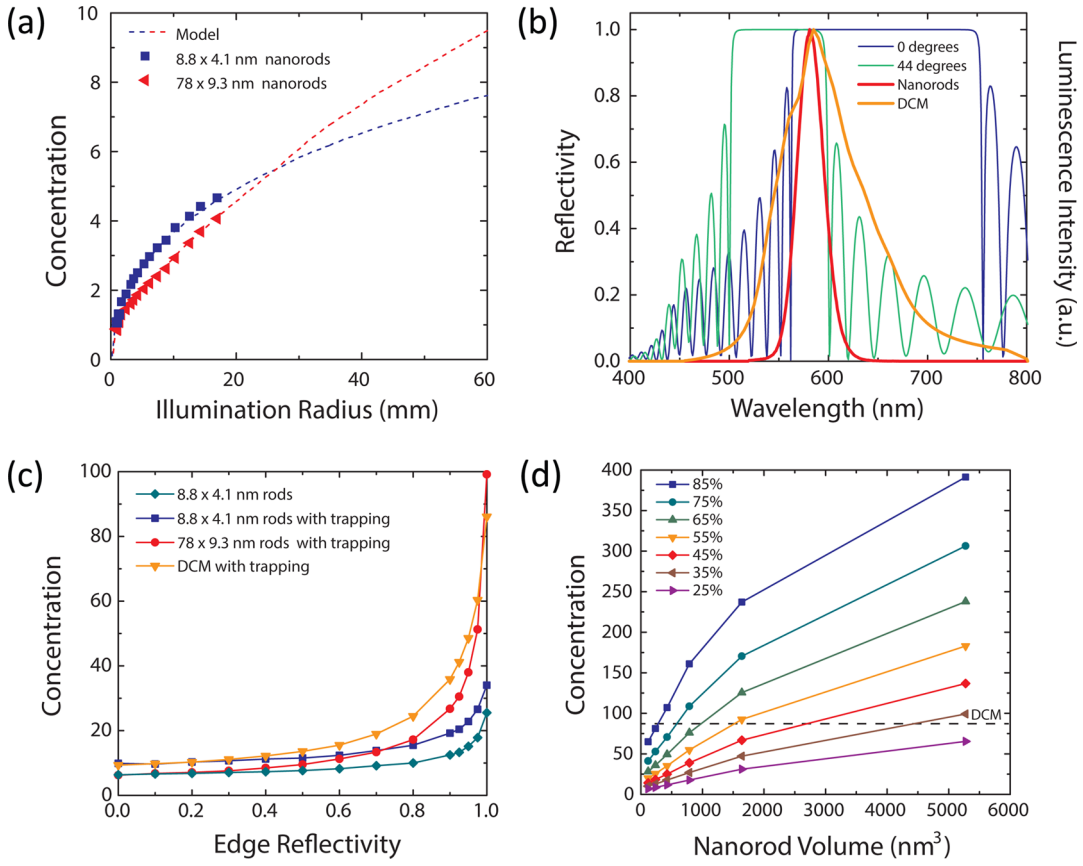

Figure 4. (a) Monte Carlo ray tracing simulation with independently measured parameters matches experimental data well and predicts that at larger device sizes the increased propagation distance of the large nanorods will dominate. (b) Reflectivity of optimized Bragg reflectors, shown at normal incidence and one degree below the angle of total internal reflection, are compared with the emission spectra of a representative nanorod sample and dicyanomethylene, a model organic dye. (c) Effect of light trapping is shown for two nanorod samples and dicyanomethylene. (d) Holding quantum yield constant for a range of quantum yields, increases in nanorod volume result in increases in photon concentration. Small nanorods require higher quantum yields than large nanorods.

cases. In contrast, the comparatively wide emission spectrum of DCM allows only 95% reflectivity. In order for the Bragg reflector to fully capture the organic dye emission, a much wider reflectance peak would be needed, necessitating unreasonably high index contrast between the two materials in the stack.

The effect of trapping the luminescence on concentration is shown in Figure 4c. Without light trapping on the edges, a luminescence trapping top surface improves the concentration factor for small nanorods from 6 to around 10. Past experimental studies have shown similar improvements for light-trapping structures optimized at normal incidence.[18,37] In our model, improving the edge reflectivity with a photonic mirror already in place on top of the LSC results in large increases in the concentration factor. Concentration factors utilizing the optimized mirror are shown in Figure 4c as the edge reflectivity is modulated from zero to unity. For small nanorods, the excessive reabsorption−re-emission limits the performance even with trapping of luminesced light. The organic dye has a luminescent quantum yield of 85%, resulting in higher concentration factors until the edge reflectivity approaches unity. At that point, the highly efficient light trapping due to the narrow emission band allows the large nanorods with their relatively low luminescent quantum yield of only 35% to achieve concentration factors of nearly 100. The combination of efficient trapping and long propagation distances reduces escape losses.

Figure 4d shows the effect of nanorod size on the concentration factor for a range of luminescent quantum yields. Others have reported luminescent quantum yields of up to 80% for the CdSe/CdS nanorod system[38,39] and 97% for the core/shell system.[25] Holding the quantum yield constant shows that, in the regime of excellent light trapping, there is a nearly linear relationship between nanorod volume and photon concentration factor. This is due to the reduced reabsorption of the larger nanorods: linear increases in volume result in linear increases in the propagation length of photons inside the LSC, resulting in more chances for the photon to be absorbed by the solar cell. As the nanorod volume gets very large, the propagation distance asymptotes due to scattering in the polymer matrix. While the simulations did not include the effects of scattering by the nanorods, this is found to be a small effect. We calculate the scattering using the electrostatic dipole

approximation (details in Supporting Information) and show that, for all the nanorods in this study, the reduced reabsorption of larger rods is more important than their increased scattering. Further increases in the nanorod volume would likely cause the scattering to overwhelm the reduced reabsorption of the larger rods and result in diminished concentration factors. Additionally, with the efficient light-trapping structure used in these simulations, larger nanorods do not require as high of luminescent quantum yields in order to outperform their organic dye counterparts.

Such high concentrations are unprecedented in the literature, and the effects of these high photon fluxes on the nanorods are not obvious. A variety of nonlinear optical and electronic effects in the nanorod lumophore may become relevant. For example, the absorption of the CdSe core exciton should saturate for large nanorods with long lifetimes at concentration factors over 100, resulting in exceptionally long propagation distances. At these high excitation levels, Auger recombination and stimulated emission may change the radiative and nonradiative rates. A thorough examination of these nonlinear effects is beyond the scope of this study.

CONCLUSION

This investigation of CdSe/CdS nanorod lumophores for luminescent solar concentration highlights design considerations for reaching the high-concentration regime. We demonstrate experimentally that increases in nanorod volume lead to increases in the propagation length of luminesced photons. We show the importance of narrow emission line widths for achieving efficient trapping of luminesced light and the importance of efficient luminescence trapping for achieving high concentration. Further, we show the trade-off between luminescence quantum yield and reabsorption once trapping is implemented, showing the necessity of lumophores with both low reabsorption and high quantum yield. We expect additional improvements to be made in the LSC device through synthesis of particles with band gaps better matched to the solar spectrum, further optimization of the LSC geometry, and the utilization of a photovoltaic cell that is well-matched to the emission of the lumophore. With the design principles shown in this paper, the high-concentration regime should be accessible.

EXPERIMENTAL SECTION

Synthesis of Seeded Nanorods. CdSe/CdS seeded nanorod synthesis was adapted from literature[39,40] with size control.[41] Details can be found in the Supporting Information.

Characterization of Seeded Nanorods. Absorption spectra were obtained on nanorods dispersed in hexanes by transmission measurements with a Shimadzu 3600 UV−vis−NIR absorption spectrometer. Emission spectra were obtained for nanorods dispersed in hexanes with a HORIBA Jobin-Yvon FluoroLog 2 spectrofluorimeter utilizing a photomultiplier tube detector. Luminescent quantum yields were obtained using a HORIBA Jobin-Yvon FluoroLog 3 spectrofluorimeter with an integrating sphere, calibrated using a NIST-traceable Avalight HAL-CAL-CC-VISNIR calibration lamp, serial number LS-1007057. Luminescence lifetime was obtained on a PicoQuant FluoTime 300 with 407 nm excitation by a LDH-P-C-405 pulsed diode laser and a PMA-175 detector. Transmission electron micrographs were obtained on a 200 kV Tecnai G220 S-TWIN with a Gatan SC200 CCD camera.

Preparation of Nanorod Dispersion in Monomer. Lauryl methacrylate (LMA) and ethylene glycol dimethacrylate (EGDMA) were purchased from Sigma Aldrich and purified over an inhibitor removing column (Sigma Aldrich product #306312) to remove the monomethyl ether of hydroquinone (MEHQ) polymerization inhibitor. LMA and EGDMA were mixed at a 10:1 ratio. Quantum rods in hexane solution, together with 4% by volume trioctylphosphine, were added to the mixture, and then the solvent was evaporated with a rotovap at 40 °C. The resultant solution is clear and stable at room temperature for an extended period of time. Photoinitiator Darocur 1173 (Sigma Aldrich) was added (1% by volume) before polymerization.

Fabrication of LSC Integrated with Si Micro Solar Cell Module. Fabrication and transfer printing of micro solar cells has been described previously.[30,31] A quartz substrate is prepared by spin-coating a 10 μm layer of partially cured UV-curable adhesive (NOA61 from Norland). The substrate and device were ozone activated in a UVOCS T10X19 OES and immediately brought into 3-(trimethoxysilyl)propyl methacrylate (Sigma Aldrich) vapor for 1 h to enhance adhesion between the PLMA and the substrate. Then 30 μm spacer soda lime glass beads (SPI product #2714) were sparsely sprinkled onto the substrate. A tridecafluoro-1,1,2,2-tetrahydrooctyl-1-trichlorosilane (Sigma Aldrich) treated quartz plate was then secured on top of the printed cell module and spacers, with treated surface facing down. Under inert atmosphere, the solution of quantum rods in monomer was then capillary-filled into the cavity with the flow parallel to the long axis of the microcell. Still in inert atmosphere, the assembly was cured for 45 min under UV illumination and then annealed at 100 °C for 30 min. The quartz top plate was then relieved, leaving the top surface of the microcell and PLMA exposed. The top contact of the device is achieved by screen-printing a silver epoxy (E4110, Epoxy Technology) line through a stencil mask formed by aligning two sloped PDMS blocks under stereoscope and curing at RT for over 48 h.

Electronic Characterization. Photovoltaic characterization was performed with a Keithley 2400 sourcemeter. The illumination source is an Oriel 91192-1000W solar simulator with AM1.5G filter. External quantum efficiency is measured using a Gooch & Housego OL-750 automated spectroradiometric system.

Conflict of Interest: The authors declare no competing financial interest.

Acknowledgment. The authors thank Eric Brueckner and Matt Small for assistance in transfer printing devices and taking STEM images. N.D.B. was supported by the National Science Foundation Graduate Research Fellowship Program under Grant No. DGE 1106400. Nanorod synthesis and characterization was supported by the Light−Material Interactions in Energy Conversion, an Energy Frontier Research Center funded by the U.S. Department of Energy, Office of Science, Office of Basic Energy Sciences, under Contract DE-AC02-05CH11231, part of the EFRC at Caltech under DE-SC0001293. Further nanorod characterization performed at the Molecular Foundry at Lawrence Berkeley National Laboratory was supported by the Office of Science, Office of Basic Energy Sciences, of the U.S. Department of Energy under Contract 396 DE-AC02-05CH11231. Device fabrication and testing at the University of Illinois at Urbana—Champaign was supported by the Light−Material Interactions in Energy Conversion, an Energy Frontier Research Center funded by the U.S. Department of Energy, Office of Science, Office of Basic Energy Sciences, under Contract 67N-1087758, part of the EFRC at Caltech under DE-SC0001293.

Supporting Information Available: Further details of the experimental methods including nanoparticle synthesis and measurement techniques, a description of the curve fitting and error analysis techniques, and a description of the optical models used in the Monte Carlo simulation are contained in the Supporting Information. This material is available free of charge *via* the Internet at http://pubs.acs.org.

REFERENCES AND NOTES

1. Goetzberger, A.; Greubel, W. Solar Energy Conversion with Fluorescent Collectors. *Appl. Phys.* **1977**, *14*, 123–139.
2. Weber, W. H.; Lambe, J. Luminescent Greenhouse Collector for Solar Radiation. *Appl. Opt.* **1976**, *15*, 2299–2300.
3. Smestad, G.; Ries, H.; Winston, R.; Yablonovitch, E. The Thermodynamic Limits of Light Concentrators. *Sol. Energy Mater.* **1990**, *21*, 99–111.
4. Yablonovitch, E. Thermodynamics of the Fluorescent Planar Concentrator. *J. Opt. Soc. Am.* **1980**, *70*, 1362–1363.
5. Würfel, P. *Physics of Solar Cells*; Wiley-VCH: Weinheim, Germany, 2005.
6. Debije, M. G.; Verbunt, P. P. C. Thirty Years of Luminescent Solar Concentrator Research: Solar Energy for the Built Environment. *Adv. Energy Mater.* **2012**, *2*, 12–35.
7. Batchelder, J. S.; Zewail, A. H.; Cole, T. Luminescent Solar Concentrators. 1 Theory of Operation and Techniques for Performance Evaluation. *Appl. Opt.* **1979**, *18*, 3090–3110.
8. Batchelder, J. S.; Zewail, A. H.; Cole, T. Luminescent Solar Concentrators. 2 Experimental and Theoretical Analysis of Their Possible Efficiencies. *Appl. Opt.* **1981**, *20*, 3733.
9. Slooff, L. H.; Bende, E. E.; Burgers, A. R.; Budel, T.; Pravettoni, M.; Kenny, R. P.; Dunlop, E. D.; Büchtemann, A. A Luminescent Solar Concentrator with 7.1% Power Conversion Efficiency. *Phys. Status Solidi Rapid Res. Lett.* **2008**, *2*, 257–259.
10. Currie, M. J.; Mapel, J. K.; Heidel, T. D.; Goffri, S.; Baldo, M. A. High-Efficiency Organic Solar Concentrators for Photovoltaics. *Science* **2008**, *321*, 226–228.
11. Yoon, J.; Li, L.; Semichaevsky, A. V.; Ryu, J. H.; Johnson, H. T.; Nuzzo, R. G.; Rogers, J. A. Flexible Concentrator Photovoltaics Based on Microscale Silicon Solar Cells Embedded in Luminescent Waveguides. *Nat. Commun.* **2011**, *2*, 343.
12. Semichaevsky, A. V.; Johnson, H. T.; Yoon, J.; Nuzzo, R. G.; Li, L.; Rogers, J. Theory for Optimal Design of Waveguiding Light Concentrators in Photovoltaic Microcell Arrays. *Appl. Opt.* **2011**, *50*, 2799–2808.
13. Sheng, X.; Shen, L.; Kim, T.; Li, L.; Wang, X.; Dowdy, R.; Froeter, P.; Shigeta, K.; Li, X.; Nuzzo, R. G.; *et al.* Doubling the Power Output of Bifacial Thin-Film Gaas Solar Cells by Embedding Them in Luminescent Waveguides. *Adv. Energy Mater.* **2013**, *3*, 991–996.
14. Earp, A. A.; Smith, G. B.; Franklin, J.; Swift, P. Optimisation of a Three-Colour Luminescent Solar Concentrator Daylighting System. *Sol. Energy Mater. Sol. Cells* **2004**, *84*, 411–426.
15. Chatten, A. J.; Barnham, K. W. J.; Buxton, B. F.; Ekins-Daukes, N. J.; Malik, M. A. Quantum Dot Solar Concentrators. In *Symposium on the Efficient Use of Solar Radiation in Photovoltaic Power Engineering*, St. Petersburg, **2003**.
16. Chatten, A. J.; Barnham, K. W. J.; Buxton, B. F.; Ekins-Daukes, N. J.; Malik, M. A. A New Approach to Modelling Quantum Dot Concentrators. *Sol. Energy Mater. Sol. Cells* **2003**, 75.
17. Debije, M. G.; Van, M.-P.; Verbunt, P. P. C.; Kastelijn, M. J.; van der Blom, R. H. L.; Broer, D. J.; Bastiaansen, C. W. M. Effect on the Output of a Luminescent Solar Concentrator on Application of Organic Wavelength-Selective Mirrors. *Appl. Opt.* **2009**, *49*, 745–751.
18. Slooff, L. H.; Burgers, A. R.; Debije, M. G. Reduction of Escape Cone Losses in Luminescent Solar Concentrators with Cholesteric Mirrors. *Proc. SPIE* **2008**, *7043*, 704306-7.
19. Alivisatos, A. P. Perspectives on the Physical Chemistry of Semiconductor Nanocrystals. *J. Phys. Chem.* **1996**, *100*, 13226–13239.
20. Alivisatos, A. P. Semiconductor Clusters, Nanocrystals, and Quantum Dots. *Science* **1996**, *271*, 933–937.
21. Bomm, J.; Büchtemann, A.; Chatten, A. J.; Bose, R.; Farrell, D. J.; Chan, N. L. A.; Xiao, Y.; Slooff, L. H.; Meyer, T.; Meyer, A.; *et al.* Fabrication and Full Characterization of State-of-the-Art Quantum Dot Luminescent Solar Concentrators. *Sol. Energy Mater. Sol. Cells* **2011**, *95*, 2087–2094.
22. Hyldahl, M. G.; Bailey, S. T.; Wittmershaus, B. P. Photostability and Performance of CdSe/ZnS Quantum Dots in Luminescent Solar Concentrators. *Sol. Energy* **2009**, *83*, 566–573.
23. Pal, B. N.; Ghosh, Y.; Brovelli, S.; Laocharoensuk, R.; Klimov, V. I.; Hollingsworth, J. A.; Htoon, H. 'Giant' CdSe/CdS Core/Shell Nanocrystal Quantum Dots as Efficient Electroluminescent Materials: Strong Influence of Shell Thickness on Light-Emitting Diode Performance. *Nano Lett.* **2012**, *12*, 331–336.
24. Chen, Y.; Vela, J.; Htoon, H.; Casson, J. L.; Werder, D. J.; Bussian, D. A.; Klimov, V. I.; Hollingsworth, J. A. Giant Multishell CdSe Nanocrystal Quantum Dots with Suppressed Blinking. *J. Am. Chem. Soc.* **2008**, *130*, 5026–5027.
25. Chen, O.; Zhao, J.; Chauhan, V. P.; Cui, J.; Wong, C.; Harris, D. K.; Wei, H.; Han, H. S.; Fukumura, D.; Jain, R. K.; *et al.* Compact High-Quality CdSe–CdS Core–Shell Nanocrystals with Narrow Emission Linewidths and Suppressed Blinking. *Nat. Mater.* **2013**, *12*, 445–451.
26. Fisher, M.; Zanella, M.; Farrell, D. J.; Manna, L.; Stavrinou, P.; Chatten, A. J. Luminescent Solar Concentrators Utilising Aligned CdSe/CdS Nanorods. In *37th IEEE Photovoltaic Specialists Conference*, Seattle, WA, **2011**.
27. She, C.; Demortière, A.; Shevchenko, E. V.; Pelton, M. Using Shape To Control Photoluminescence from CdSe/CdS Core/Shell Nanorods. *J. Phys. Chem. Lett.* **2011**, *2*, 1469–1475.
28. Lee, J.; Sundar, V. C.; Heine, J. R.; Bawendi, M. G.; Jensen, K. F. Full Color Emission from II-VI Semiconductor Quantum Dot–Polymer Composites. *Adv. Mater.* **2000**, *12*, 1102–1105.
29. Bomm, J.; Buchtemann, A.; Fiore, A.; Manna, L.; Nelson, J. H.; Hill, D.; van Sark, W. G. Fabrication and Spectroscopic Studies on Highly Luminescent CdSe/CdS Nanorod Polymer Composites. *Beilstein J. Nanotechnol.* **2010**, *1*, 94–100.
30. Yoon, J.; Baca, A. J.; Park, S. I.; Elvikis, P.; Geddes, J. B., III; Li, L.; Kim, R. H.; Xiao, J.; Wang, S.; Kim, T. H.; *et al.* Ultrathin Silicon Solar Microcells for Semitransparent, Mechanically Flexible and Microconcentrator Module Designs. *Nat. Mater.* **2008**, *7*, 907–915.
31. Yao, Y.; Brueckner, E.; Li, L.; Nuzzo, R. Fabrication and Assembly of Ultrathin High-Efficiency Silicon Solar Microcells Integrating Electrical Passivation and Anti-reflection Coatings. *Energy Environ. Sci.* **2013**, *6*, 3071.
32. Ninomiya, S.; Adachi, S. Optical Properties of Wurtzite. *J. Appl. Phys.* **1995**, *78*, 1183–1190.
33. Yablonovitch, E. Statistical Ray Optics. *Opt. Soc. Am.* **1982**, *72*, 899–907.
34. Debije, M. G.; Teunissen, J.-P.; Kastelijn, M. J.; Verbunt, P. P. C.; Bastiaansen, C. W. M. The Effect of a Scattering Layer on the Edge Output of a Luminescent Solar Concentrator. *Sol. Energy Mater. Sol. Cells* **2009**, *93*, 1345–1350.
35. Earp, A. A.; Smith, G. B.; Swift, P. D.; Franklin, J. Maximising the Light Output of a Luminescent Solar Concentrator. *Sol. Energy* **2004**, *76*, 655–667.
36. Ferry, V. E.; Verschuuren, M. A.; Lare, M. C.; Schropp, R. E.; Atwater, H. A.; Polman, A. Optimized Spatial Correlations for Broadband Light Trapping Nanopatterns in High Efficiency Ultrathin Film a-Si:H Solar Cells. *Nano Lett.* **2011**, *11*, 4239–4245.
37. Goldschmidt, J. C.; Peters, M.; Bösch, A.; Helmers, H.; Dimroth, F.; Glunz, S. W.; Willeke, G. Increasing the Efficiency of Fluorescent Concentrator Systems. *Sol. Energy Mater. Sol. Cells* **2009**, *93*, 176–182.
38. Talapin, D. V.; Koeppe, R.; Götzinger, S.; Kornowski, A.; Lupton, J. M.; Rogach, A. L.; Benson, O.; Feldmann, J.; Weller, H. Highly Emissive Colloidal CdSe/CdS Heterostructures of Mixed Dimensionality. *Nano Lett.* **2003**, *3*, 1677–1681.

39. Talapin, D. V.; Nelson, J. H.; Shevchenko, E. V.; Aloni, S.; Sadtler, B.; Alivisatos, A. P. Seeded Growth of Highly Luminescent CdSe/CdS Nanoheterostructures with Rod and Tetrapod Morphologies. *Nano Lett.* **2007**, *7*, 2951–2959.
40. Carbone, L.; Nobile, C.; Giorgi, M. D.; Sala, F. D.; Morello, G.; Pompo, P.; Hytch, M.; Snoeck, E.; Fiore, A.; Franchini, I. R.; *et al.* Synthesis and Micrometer-Scale Assembly of Colloidal CdSe/CdS Nanorods Prepared by a Seeded Growth Approach. *Nano Lett.* **2007**, *7*, 2942–2950.
41. Jain, P. K.; Amirav, L.; Aloni, S.; Alivisatos, A. P. Nanoheterostructure Cation Exchange Anionic Framework Conservation. *J. Am. Chem. Soc.* **2010**, *132*, 9997–9999.